The antiphase boundary in half-metallic Heusler alloy $Co_2Fe(Al,Si)$: atomic structure, spin polarization reversal, and domain wall effects

Zlatko Nedelkoski, Ana M. Sanchez, Arsham Ghasemi, Kohei Hamaya, Richard F. L. Evans, Gavin R. Bell, Atsufumi Hirohata, and Vlado K. Lazarov

Citation: Appl. Phys. Lett. **109**, 222405 (2016); doi: 10.1063/1.4971281
View online: http://dx.doi.org/10.1063/1.4971281
View Table of Contents: http://aip.scitation.org/toc/apl/109/22
Published by the American Institute of Physics

The antiphase boundary in half-metallic Heusler alloy $Co_2Fe(Al,Si)$: atomic structure, spin polarization reversal, and domain wall effects

Zlatko Nedelkoski,[1] Ana M. Sanchez,[2] Arsham Ghasemi,[1] Kohei Hamaya,[3] Richard F. L. Evans,[1] Gavin R. Bell,[2] Atsufumi Hirohata,[4] and Vlado K. Lazarov[1,a)]
[1]*Department of Physics, University of York, York YO10 5DD, United Kingdom*
[2]*Department of Physics, University of Warwick, Coventry CV4 7AL, United Kingdom*
[3]*Center for Spintronics Research Network, Osaka University, Osaka 560-8531, Japan*
[4]*Department of Electronics, University of York, York YO10 5DD, United Kingdom*

(Received 14 October 2016; accepted 9 November 2016; published online 2 December 2016)

Atomic resolution scanning transmission electron microscopy reveals the presence of an antiphase boundary in the half-metallic $Co_2Fe(Al,Si)$ full Heusler alloy. By employing the density functional theory calculations, we show that this defect leads to reversal of the sign of the spin-polarization in the vicinity of the defect. In addition, we show that this defect reduces the strength of the exchange interactions, without changing the ferromagnetic ordering across the boundary. Atomistic spin calculations predict that this effect reduces the width of the magnetic domain wall compared to that in the bulk. *Published by AIP Publishing*. [http://dx.doi.org/10.1063/1.4971281]

Density functional theory (DFT) calculations predict 100% spin-polarization (SP) at the Fermi-level, i.e., half-metallic character, for a number of Co-based full Heusler alloys such as $Co_2Fe(Al,Si)$ (CFAS), Co_2FeSi (CFS), and Co_2MnSi (CMS).[1–3] Due to this desirable property for spintronic applications, they have been attracting significant theoretical as well as experimental research interest and already have been used as a functional part in spin-valves and magnetic tunnelling junctions.[4–7] CFAS is the most promising candidate from this group, since besides their common properties such as half-metallicity and very high Curie temperature, it has a mid-gap Fermi-level which in turn makes CFAS more robust against temperature effects.[8,9]

Although the ideal bulk structures are predicted half-metallic materials, number of theoretical and experimental studies have shown that the desirable spin-electronic properties can be significantly affected by the presence of disorder, strain, and variations of the stoichiometry.[10–13] Moreover, in real devices, they are in the form of thin films interfaced with a substrate or neighbouring layer where the interface itself can destroy the local SP.[14–19] This in turn can significantly decrease the overall device performance (e.g., their magnetoresistance for spin-valves) or lead to inefficient spin-injection in halfmetal/semiconductor heterostructures. Hence the understanding of their atomic structure and how it influences the electronic/magnetic properties is crucial in order to fully utilise the significant potential of these materials for spintronic applications.

In this letter we show that antiphase boundaries (APB) form in CFAS films. By employing aberration-corrected high-angle-annular-dark-field (HAADF) scanning transmission electron microscopy (STEM), we reveal the exact atomic structure of the $\frac{1}{4}a[111]$ APB structural defect and create a realistic atomistic model. This model was used for the electronic structure calculations by DFT. The DFT calculations show that these structural defects do not affect the preference for ferromagnetic (FM) ordering, in other words, the grains across the boundary are still ferromagnetically coupled. In contrast, the widely present APBs in oxide halfmetals (e.g., magnetite) significantly affect the magnetic state of the film due to the presence of very strong antiferromagnetic (AFM) interactions across these defects.[20] Although the interactions across the APB keep the FM character, we show that their strength is significantly decreased which can lead to reduction of magnetic domain wall width. In addition, the layer-by-layer spin-polarized partial density of states (PDOS), demonstrate that the local spin-polarisation is reversed i.e., electronic states that are negatively spin polarised at the Fermi-level dominate the electronic properties of the boundary. Finally, we show that the formation energy of the experimentally observed APB is $0.9\,J/m^2$, which is almost an order of magnitude higher compared to APBs in Fe_3O_4.

The sample was prepared by co-deposition of Co, Fe, Si, and Al using low-temperature molecular beam epitaxy.[21,22] 18 nm-thick CFAS film was deposited on a pre-cleaned $10 \times 10\,mm^2$ Ge (111) substrate at room temperature. Prior to loading Ge(111) substrates into the chamber, their surfaces were chemically cleaned with an aqueous 1% HF solution to remove any native oxide and contamination. Cross-sectional transmission electron microscopy samples were prepared by conventional methods[23] which include mechanical thinning by polishing and finishing with Ar-ion milling, as well as by Focused-Ion-Beam (FIB).[24] Atomic-level STEM analysis was performed using ARM200F microscope with probe and image aberration CEOS correctors, operating at 200 kV. Annular dark field images were obtained using a JEOL annular field detector in the range 70–280 mrad; imaging probe of ~23 pA and convergence semi-angle of ~22 mrad.

DFT calculations were performed with the CASTEP code[25] using periodically repeating supercells which contain two equivalent APBs. The PBE (Perdew–Burke–Ernzerhof) + U exchange-correlation functional[26] was used, where the Hubbard-U term was set to 2.1 eV for both d-block elements,

a)Email: vlado.lazarov@york.ac.uk

Co and Fe.[27] This value for the Hubbard-U term has previously been shown to open up the minority band-gap, approximately correcting for the delocalising effect of self-interaction with PBE alone.[28] The plane wave cut-off energy was set to 600 eV, while the Brillouin zone was sampled using a Monkhorst-Pack grid with a *k*-point sampling spacing of 0.03 2πÅ^{-1}. The atomic coordinates were fully geometry optimized. The spin-polarized PDOS were calculated with the OPTADOS[29] code using the fixed Gaussian broadening scheme.

Atomistic spin dynamics simulations were performed using the VAMPIRE code[30] with Heisenberg exchange and uniaxial anisotropy energy. For the anisotropy we use a value of 20 kJ/m^3 (Ref. 31) and the anisotropy axis is set along the [11–2] direction as discussed in Ref. 32. The near neighbors exchange interaction energies are taken from ab-initio calculations[33] with the interatomic distance given in parentheses in lattice units: Mn-Co(0.43) = 2.80 mRy; Co-Co(0.50) = 0.75 mRy; Mn-Mn(0.70) = 0.35 mRy; Co-Co(0.86) = 0.30 mRy. The constructed supercells for the atomistic magnetic simulations have dimensions of $\sim 16 \times 16 \times 280$ nm.

Figure 1(a) is an atomic resolution HAADF STEM image of a film region that contains the structural defect where the boundary plane is labelled with the white dashed line. On either side of the boundary plane left or right, the HAADF imaging shows distinctive bright-dark contrast for the atomic planes along the [001] direction. The bright contrast corresponds to Co atomic columns while the darker to the Fe-Si/Al atomic columns, as expected for *B2* ordered film (see supplementary material). For *B2* ordering we would expect the following atomic plane stacking sequence… Co-(Fe-Si/Al)-Co-(Fe-Si/Al)… along the [111] crystallographic direction which is exactly what is observed in the Figure 1(a).

This distinctive atomic column stacking pattern is disrupted at the boundary plane, as observed by following the atomic columns in the (001) plane (outlined by the yellow dashed rectangle). By considering the (001) atomic plane across the boundary, we can see that the positions of Co atomic columns switch to Fe-(Si/Al) atomic columns. The same observation applies for the (111) atomic planes, i.e., by following the atomic columns (outlined by the white dashed rectangle) the Fe-(Si/Al) atomic columns are switched to Co across the APB. This discontinuity of Co and Fe-Si/Al columns on a same atomic plane, is further demonstrated by the Fourier filtered images, Figures 1(b) and 1(c). The atomic planes shift along the [111] direction can be easily observed in Figure 1(c) since the selected diffraction spot (yellow circle) filters every second (001) atomic plane. By following the yellow dashed rectangle oriented along a (001) atomic plane, right of the APB, it shows an atomic plane, while on the left, the atomic plane is shifted for $^1/_4a$[111], where *a* is the lattice constant of CFAS.

In the Figure 2(a) we show the atomistic model derived from the atomic resolution HAADF images. The model consists of two bulk-like CFAS regions shifted for $^1/_4a$[111], i.e., a shift of three (111) atomic planes along the [111] crystallographic direction. First we discuss the effect of the APB on the local SP in the APB vicinity. For clarity, the region in the vicinity of the boundary has been divided into seven different blocks labelled as *L3′, L2′, L1′, L0, L1, L2, L3* (Figure 2(a)). The corresponding spin-polarized PDOS at the boundary (region *L0*) and the next three neighbouring bilayers (*L1*, *L2*, and *L3*) are shown, Figure 2(b). *L1′*, *L2′*, and *L3′* do not differ from *L1*, *L2*, and *L3* due to the symmetries in the supercell, hence they are not shown. The results clearly show that the effect of the APB is very localised. At the APB (layer *L0*), there are significant number of spin-down states which cause this region to be inversely spin-polarized (SP = −44%) compared to the bulk-like part of the electrode. As we move away from the structural defect, the SP recovers; *L1* has SP = +4% while from *L2, L3* onwards, the properties become bulk-like. Note that the layers *L2* and *L3* already show proper band gap for the minority (spin down) electrons, as expected for bulk CFAS.

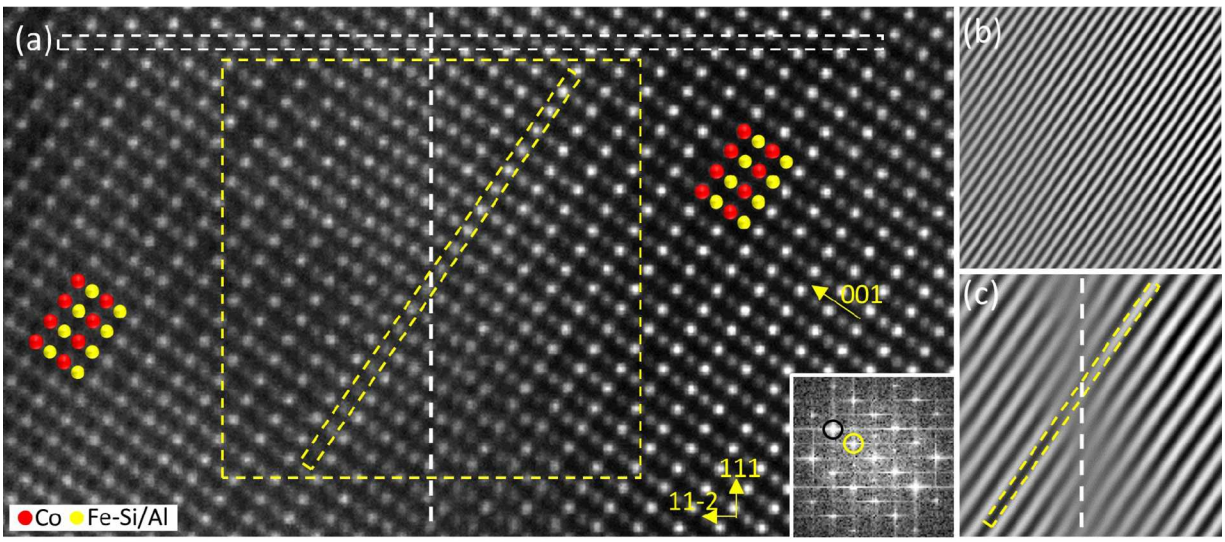

FIG. 1. Atomic resolution STEM image at the APB defect acquired along the [1-10] zone axis. The defect plane is labelled with a dashed white line; dashed white rectangle is along a (111) plane; dashed yellow rectangle along a (001) atomic plane. The colour coding of the overlaid structural model is given in the legend. Fast Fourier transform of the area within the yellow dashed square is shown as inset and used to construct the filtered images in (b) using the spot marked with a black circle and (c) with the spot marked with a yellow circle; both are [001] type diffraction spots.

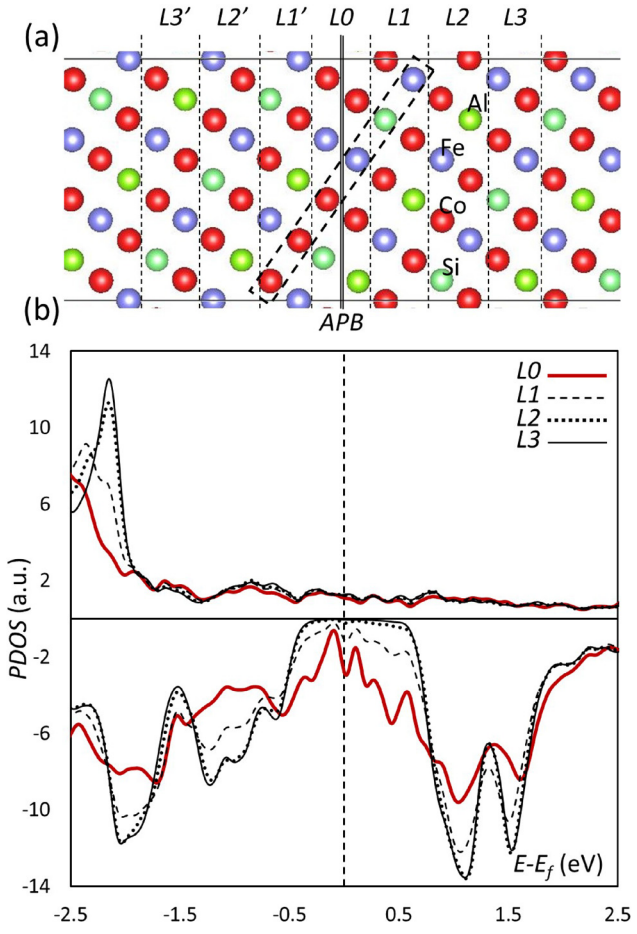

FIG. 2. (a) Structural model of the APB viewed along the [1-10] projection. The vertical direction corresponds to [111]; (001) plane is along the black dashed rectangle; boundary plane is labelled with the double solid line, while the dashed lines are used to separate the supercell into seven blocks used to plot the spin-polarized PDOS shown in (b) where spin-up states are shown in the upper part; spin-down in the bottom part of the plot.

In order to find out whether the SP-reversal is dependent on the chemical composition of the full Co-based Heusler alloys, we consider the effect of the APB on the example of CFS and CMS. Figure S1 of supplementary material shows that at the boundary vicinity, in both cases, there is a significant change of density of states around the Fermi-level. While in CFS, similarly to CFAS the SP is reversed, in CMS the SP keeps the positive sign at the Fermi-level, however the band gap is drastically reduced. These calculations all show that the APBs in Co-based Heusler alloys of form $Co_2(Fe,Mn)(Si,Al)$ can be very detrimental for the spin-electronic structure of the electrode. This may be a particularly strong effect for planar device geometries since the APBs can act as extended regions for spin scattering events.

Next we consider the strength of the exchange interactions between atoms across the APB. The exchange constants are proportional to the energy required to transform the FM alignment into an AFM one, and in full Co-based Heusler alloys are defined for pairs of two atoms. For example, for CMS: Co-Co, Mn-Co, and Mn-Mn bonds have characteristic values of the exchange interaction constants which in turn define the general magnetic behaviour of these materials such as their Curie temperature (T_c). First-principles calculations of exchange constants is not a trivial problem, however, it has been done for simplistic systems, including the bulk CMS.[33] By using the bulk values reported in Ref. 33 and performing DFT calculations for the energy differences between the AFM and FM states in the presence of APB, we have calculated the average strength of the exchange interactions across the APB defect.

First we construct four supercells with the same size and number of atoms. The first two are bulk CFAS supercells; one of them has all magnetic moments aligned along the same direction, while the other one is divided into two halves with an opposite magnetic moment alignment. As expected, the AFM coupled supercell has a higher total energy by $0.73\,J/m^2$ with respect to the FM supercell. Performing the same calculations on a supercell with an APB in the middle, we find that the ferromagnetic alignment between the two halves is still favoured, but with a smaller energy difference between the AFM and FM configuration ($0.49\,J/m^2$). These results imply that the exchange interactions are significantly weakened across the APB defect. Table I shows the total energy differences between AFM and FM configurations for the considered supercells. The same analysis has been also performed for CFS and CMS. As can be seen from Table I, the reduction of exchange interactions strength across the APB is most pronounced for CMS (where they are weakened by a factor of $\sim$3).

The reduced exchange interactions across the APBs can affect the width of the magnetic domain wall in Heuslers films. One can estimate this effect assuming that the average exchange constants across the APB are known. Exchange interactions are strongly localised decaying very steeply as the inter-atomic distance increases, as shown for the bulk CMS.[33] By performing atomistic magnetic simulations (Figure S2 of supplementary material) we show that a good value of the Curie temperature (slightly above 900 K) can be obtained (the measured one is 985 K) even by taking into account only the first four shortest interactions for CMS. Figure S3 of supplementary material presents an overview of the bond types across the APB defect as a function of the inter-atomic distance. In order to estimate the value of the shortest exchange interactions appearing across the APB, we use the following method. We assign to the shortest three interactions an equal value of J which is to be determined. By varying the J in a given range, for each value of J, the energy difference between the AFM and FM state is calculated. Knowing (from DFT calculations) that the energy difference between AFM and FM is 0.9 eV, an average value of $J = 0.6$ mRy has been obtained, Figure S4 of supplementary material.

By using this J value at the APB, we have performed magnetic atomistic simulations and calculated the change in

TABLE I. Energy differences for CFAS, CFS, and CMS models. E_{form} stands for the APB formation energies, $E^{AFM}_{bulk} - E^{FM}_{bulk}$ is the energy difference between the AFM and FM bulk models; while $E^{AFM}_{APB} - E^{FM}_{APB}$ is the same quantity but for APB supercell models.

Structure	$E^{AFM}_{bulk} - E^{FM}_{bulk}$ (J/m^2)	$E^{AFM}_{APB} - E^{FM}_{APB}$ (J/m^2)	E_{form} (J/m^2)
CFAS	0.73	0.49	0.90
CFS	0.62	0.30	0.92
CMS	0.53	0.18	1.14

the magnetic domain wall width in a presence of an APB. The magnetic moments were initially set in opposite directions at each half of the large supercell model (the APB is in the centre). The whole system is allowed to relax until a convergence is obtained, Figures 3(a) and 3(b). Figure 3(c) shows that the effect of the APB is small but noticeable. The magnetization (M_z) in the presence of APB decreases slightly faster in comparison to the bulk. The domain wall width for the bulk (with chosen parameters given in the methods section) is ~150 nm. The presence of the APB reduces the domain wall width by about ~25 nm, as a result of the weakened exchange interactions.

The presented results show that the APB's influence on overall magnetic properties of Co-based Heuslers is not as dramatic as in the materials systems with super-exchange interactions i.e., ferrimagnetic oxides (e.g., magnetite) where the nature of the bonding changes across the APB (e.g., from FM to strong AFM).

Finally we calculate the formation energies of the $^1/_4a$[111] APBs in CFAS, CMS, and CFS. For CFAS, the APB formation energy has been found to be 0.9 J/m^2 by comparing the total energies of APB and bulk supercells. The values are very similar for an APB in CFS and CMS where we obtain 0.92 J/m^2 and 1.14 J/m^2, respectively, as shown in Table I. These energies are about an order of magnitude higher compared to the formation energy of the APB present in magnetite.[20] The close proximity of the step in the substrate surface (shown in Figure S5 of supplementary material) and the APB in the film, indicates that a step on the Ge (111) surface can act as a nucleation centre for APB formation.

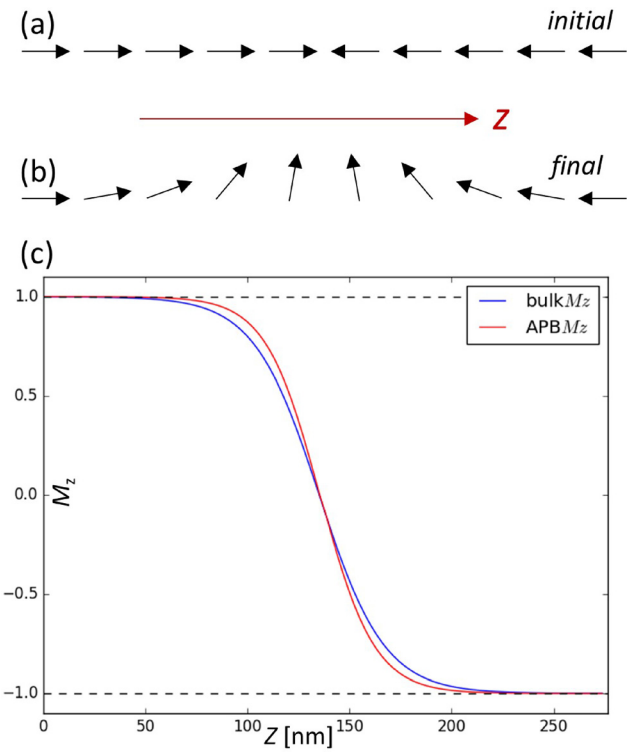

FIG. 3. Schematics of the (a) initial (b) final magnetic configuration used to calculate the width of the magnetic domain wall for both bulk and APB models as shown in (c) where the normalised magnetization is plotted as a function of the distance along the longest dimension of the supercell.

In summary, we showed that APBs structural defects can form in thin films of Co-based full Heusler alloys. By performing DFT calculations, we have demonstrated that the defect brings a significant density of states in the minority spin band gap and for the case of CFAS, this reverses the spin-polarization. These calculations also have shown that the ferromagnetic alignment remains when an APB is introduced, although the exchange interactions across the defect are significantly weakened. By employing atomistic magnetic simulations, we showed that this weakening of the exchanges causes a slight reduction of the magnetic domain wall width. Finally, this work demonstrates that the APB defects can have considerable effects on the spin-electronic properties and their presence has to be minimized in order to fully exploit the half-metallic character of the electrode especially for planar type of spintronic devices.

See supplementary material for brief explanation of the atomic structure of bulk CFAS with $L2_1$ and $B2$ structural ordering, PDOS across the APB in CFS and CMS, Curie temperature simulations for bulk CMS, bonding analysis across the studied APB, determination of the exchange constant at the APB, as well as the HAADF STEM image which demonstrates that a step in the Ge(111) surface can act as a nucleation centre for APB formation.

This work was funded by the Engineering and Physical Sciences Research Council (EPSRC) through Grant Nos. EP/K03278X/1 and EP/K032852/1. The authors are grateful for computational support from the UK national High Performance Computing service ARCHER.

Data Availability. All data created during this research are available by request from the University of York Data Catalogue, https://dx.doi.org/10.15124/b904b99f-4d0d-47b3-864b-0b6977b7ec99.

[1]C. Felser, G. H. Fecher, and B. Balke, "Spintronics: A challenge for materials science and solid-state chemistry," Angew. Chem., Int. Ed. **46**, 668 (2007).
[2]M. I. Katsnelson, V. Y. Irkhin, L. Chioncel, A. I. Lichtenstein, and R. A. de Groot, "Half-metallic ferromagnets: From band structure to many-body effects," Rev. Mod. Phys. **80**, 315 (2008).
[3]A. Hirohata, J. Sagar, L. Lari, L. Fleet, and V. Lazarov, "Heusler-alloy films for spintronic devices," Appl. Phys. A **111**, 423 (2013).
[4]Y. Sakuraba, M. Hattori, M. Oogane, Y. Ando, H. Kato, A. Sakuma, T. Miyazaki, and H. Kubota, "Giant tunneling magnetoresistance in Co_2MnSi/Al–O/Co_2MnSi magnetic tunnel junctions," Appl. Phys. Lett. **88**, 192508 (2006).
[5]T. Ishikawa, T. Marukame, H. Kijima, K.-I. Matsuda, T. Uemura, M. Arita, and M. Yamamoto, "Spin-dependent tunneling characteristics of fully epitaxial magnetic tunneling junctions with a full-Heusler alloy Co_2MnSi thin film and a MgO tunnel barrier," Appl. Phys. Lett. **89**, 192505 (2006).
[6]S. Tsunegi, Y. Sakuraba, M. Oogane, K. Takanashi, and Y. Ando, "Large tunnel magnetoresistance in magnetic tunnel junctions using a Co_2MnSi Heusler alloy electrode and a MgO barrier," Appl. Phys. Lett. **93**, 112506 (2008).
[7]T. Furubayashi, K. Kodama, H. Sukegawa, Y. K. Takahashi, K. Inomata, and K. Hono, "Current-perpendicular-to-plane giant magnetoresistance in spin-valve structures using epitaxial $Co_2FeAl_{0.5}Si_{0.5}$/Ag/$Co_2FeAl_{0.5}Si_{0.5}$ trilayers," Appl. Phys. Lett. **93**, 122507 (2008).
[8]R. Shan, H. Sukegawa, W. H. Wang, M. Kodzuka, T. Furubayashi, T. Ohkubo, S. Mitani, K. Inomata, and K. Hono, "Demonstration of half-metallicity in fermi-level-tuned heusler alloy $Co_2FeAl_{0.5}Si_{0.5}$ at room temperature," Phys. Rev. Lett. **102**, 246601 (2009).

[9]J. D. Aldous, C. W. Burrows, A. M. Sánchez, R. Beanland, I. Maskery, M. K. Bradley, M. dos Santos Dias, J. B. Staunton, and G. R. Bell, "Cubic MnSb: Epitaxial growth of a predicted room temperature half-metal," Phys. Rev. B **85**, 060403 (2012).
[10]Y. Sakuraba, T. Iwase, K. Saito, S. Mitani, and K. Takanashi, "Enhancement of spin-asymmetry by $L2_1$-ordering in Co_2MnSi/Cr/Co_2MnSi current-perpendicular-to-plane magnetoresistance devices," Appl. Phys. Lett. **94**, 012511 (2009).
[11]S. Picozzi and A. J. Freeman, "Polarization reduction in half-metallic Heusler alloys: The effect of point defects and interfaces with semiconductors," J. Phys.: Condens. Matter **19**, 315215 (2007).
[12]S. Picozzi, A. Continenza, and A. J. Freeman, "Role of structural defects on the half-metallic character of Co_2MnGe and Co_2MnSi Heusler alloys," Phys. Rev. B **69**, 094423 (2004).
[13]P. Hasnip, C. Loach, J. Smith, M. Probert, D. Gilks, J. Sizeland, L. Lari, J. Sagar, K. Yoshida, M. Oogane, A. Hirohata, and V. Lazarov, "The effect of cobalt-sublattice disorder on spin polarisation in $Co_2Fe_xMn_{1-x}Si$ Heusler alloys," Materials **7**, 1473 (2014).
[14]T. M. Nakatani, T. Furubayashi, S. Kasai, H. Sukegawa, Y. K. Takahashi, S. Mitani, and K. Hono, "Bulk and interfacial scatterings in current-perpendicular-to-plane giant magnetoresistance with $Co_2Fe(Al_{0.5}Si_{0.5})$ Heusler alloy layers and Ag spacer," Appl. Phys. Lett. **96**, 212501 (2010).
[15]V. K. Lazarov, K. Yoshida, J. Sato, P. J. Hasnip, M. Oogane, A. Hirohata, and Y. Ando, "The effect of film and interface structure on the transport properties of Heusler based current-perpendicular-to-plane spin valves," Appl. Phys. Lett. **98**, 242508 (2011).
[16]L. Lari, K. Yoshida, P. L. Galindo, J. Sato, J. Sizeland, D. Gilks, G. M. Uddin, Z. Nedelkoski, P. J. Hasnip, A. Hirohata, M. Oogane, Y. Ando, and V. K. Lazarov, "Correlations between atomic structure and giant magnetoresistance ratio in Co_2(Fe,Mn)Si spin valves," J. Phys. D: Appl. Phys. **47**, 322003 (2014).
[17]Z. Nedelkoski, P. J. Hasnip, A. M. Sanchez, B. Kuerbanjiang, E. Higgins, M. Oogane, A. Hirohata, G. R. Bell, and V. K. Lazarov, "The effect of atomic structure on interface spin-polarization of half-metallic spin valves: Co_2MnSi/Ag epitaxial interfaces," Appl. Phys. Lett. **107**, 212404 (2015).
[18]B. Kuerbanjiang, Z. Nedelkoski, D. Kepaptsoglou, A. Ghasemi, S. E. Glover, S. Yamada, T. Saerbeck, Q. M. Ramasse, P. J. Hasnip, T. P. A. Hase, G. R. Bell, K. Hamaya, A. Hirohata, and V. K. Lazarov, "The role of chemical structure on the magnetic and electronic properties of $Co_2FeAl_{0.5}Si_{0.5}$/Si(111) interface," Appl. Phys. Lett. **108**, 172412 (2016).
[19]Z. Nedelkoski, D. Kepaptsoglou, A. Ghasemi, B. Kuerbanjiang, P. J. Hasnip, S. Yamada, K. Hamaya, Q. M. Ramasse, A. Hirohata, and V. K. Lazarov, "Controlling the half-metallicity of Heusler/Si(111) interfaces by a monolayer of Si–Co–Si," J. Phys.: Condens. Matter **28**, 395003 (2016).
[20]K. P. McKenna, F. Hofer, D. Gilks, V. K. Lazarov, C. Chen, Z. Wang, and Y. Ikuhara, "Atomic-scale structure and properties of highly stable antiphase boundary defects in Fe_3O_4," Nat. Commun. **5**, 5740 (2014).
[21]S. Yamada, K. Tanikawa, S. Oki, M. Kawano, M. Miyao, and K. Hamaya, "Improvement of magnetic and structural stabilities in high-quality $Co_2FeSi_{1-x}Al_x$/Si heterointerfaces," Appl. Phys. Lett. **105**, 071601 (2014).
[22]K. Tanikawa, S. Oki, S. Yamada, M. Kawano, M. Miyao, and K. Hamaya, "High-quality $Co_2FeSi_{0.5}Al_{0.5}$/Si heterostructures for spin injection in silicon spintronic devices," Thin Solid Films **557**, 390 (2014).
[23]L. Lari, S. Lea, C. Feeser, B. W. Wessels, and V. K. Lazarov, "Ferromagnetic InMnSb multi-phase films study by aberration-corrected (scanning) transmission electron microscopy," J. Appl. Phys. **111**, 07C311 (2012).
[24]A. Ghasemi, D. Kepaptsoglou, L. J. Collins-McIntyre, Q. Ramasse, T. Hesjedal, and V. K. Lazarov, "Atomic-level structural and chemical analysis of Cr-doped Bi_2Se_3 thin films," Sci. Rep. **6**, 26549 (2016).
[25]J. Clark Stewart, M. D. Segall, C. J. Pickard, P. J. Hasnip, M. I. J. Probert, K. Refson, and M. C. Payne, "First principles methods using CASTEP," Z. Kristallogr. **220**, 567 (2005).
[26]J. P. Perdew, K. Burke, and M. Ernzerhof, "Generalized gradient approximation made simple," Phys. Rev. Lett. **77**, 3865 (1996).
[27]S. Chadov, G. H. Fecher, C. Felser, J. Minár, J. Braun, and H. Ebert, "Electron correlations in $Co_2Mn_{1-x}Fe_xSi$ Heusler compounds," J. Phys. D: Appl. Phys. **42**, 084002 (2009).
[28]P. J. Hasnip, J. H. Smith, and V. K. Lazarov, "Ab initio studies of disorder in the full Heusler alloy $Co_2Fe_xMn_{1-x}Si$," J. Appl. Phys. **113**, 17B106 (2013).
[29]A. J. Morris, R. J. Nicholls, C. J. Pickard, and J. R. Yates, "OptaDOS: A tool for obtaining density of states, core-level and optical spectra from electronic structure codes," Comput. Phys. Commun. **185**, 1477 (2014).
[30]R. F. L. Evans, W. J. Fan, P. Chureemart, T. A. Ostler, M. O. A. Ellis, and R. W. Chantrell, "Atomistic spin model simulations of magnetic nanomaterials," J. Phys.: Condens. Matter **26**, 103202 (2014).
[31]T. Simon, G. Oksana, H. Jaroslav, and H. Burkard, "Magnetic anisotropy, exchange and damping in cobalt-based full-Heusler compounds: an experimental review," J. Phys. D: Appl. Phys. **43**, 193001 (2010).
[32]M. Zander, J. Herfort, K. Kumakura, H. P. Schönherr, and A. Trampert, "Epitaxial Heusler alloy Co_2FeSi films on Si(1 1 1) substrates grown by molecular beam epitaxy," J. Phys. D: Appl. Phys. **43**, 305004 (2010).
[33]M. Ležaić, P. Mavropoulos, G. Bihlmayer, and S. Blügel, "Exchange interactions and local-moment fluctuation corrections in ferromagnets at finite temperatures based on noncollinear density-functional calculations," Phys. Rev. B **88**, 134403 (2013).